$+\zeta_{2t}$), integrals $m = 1, 3$ for $W_2 < W_1$ in Table II vanish, and integral $m = 2$ may be developed as follows:

$$F_{12}^a(\zeta_{12}) = \lim_{\epsilon \to 0} \int_{\zeta_{12}+1/2(\zeta_1-\zeta_2)-\epsilon}^{\zeta_{12}+1/2(\zeta_1-\zeta_2)+\epsilon}$$

$$\times U_1(\zeta_{12}+\Delta)U_2(\zeta_{12}-\Delta)\,d\Delta , \qquad (23)$$

$$F_{12}^a(\zeta_{12}) = \lim_{\epsilon \to 0} U_1[2\zeta_{12}+\tfrac{1}{2}(\xi_1-\xi_2)]$$

$$\times \int_{-\epsilon}^{\epsilon} U_2[-\tfrac{1}{2}(\xi_1-\xi_2)-\Delta]\,d\Delta , \qquad (24)$$

$$F_{12}^a(\zeta_{12}) = U_1[2\zeta_{12}+\tfrac{1}{2}(\xi_1-\xi_2)] . \qquad (25)$$

In these expressions ζ_{12} continues to be the energy

half-way between the energies of the two electrons involved in the process, one of which is always at $\zeta_{12} = -\tfrac{1}{2}(\xi_1 - \xi_2)$. The variable change from ζ_{12} to E appropriate to this special case is also given by Eq. (19). Putting this into Eq. (25), we obtain

$$F_{12}^a(\zeta_{12}) = U_1(E_i' - E - \tfrac{1}{2}\xi_1 - \tfrac{3}{2}\xi_2) , \qquad (26)$$

which shows that F_{12}^a is not a fold at all but is the U_1 function shifted to higher energy and expanded in energy by a factor of 2. Equations (18)–(20) apply to this case as well, showing that the shift $(\Delta_1 + \Delta_2)$ in Figs. 5 and 6 is equal to $(\xi_1 - \xi_2)$. The ionization energy of the metastable level $(E_i' - E_x')$ in Fig. 5 is equal to ξ_2.

[1]H. D. Hagstrum and G. E. Becker, preceding paper, Phys. Rev. B **8**, 1580 (1973).

[2]H. D. Hagstrum, Phys. Rev. **150**, 495 (1966).

[3]H. D. Hagstrum and G. E. Becker, Phys. Rev. B **4**, 4187 (1971).

[4]H. D. Hagstrum and G. E. Becker, Phys. Rev. **159**, 572 (1967).

[5]H. D. Hagstrum and G. E. Becker, J. Chem. Phys. **54**, 1015 (1971).

[6]G. E. Becker and H. D. Hagstrum, Surf. Sci. **30**, 505 (1972).

[7]H. D. Hagstrum, Phys. Rev. **96**, 336 (1954).

[8]H. D. Hagstrum, Y. Takeishi, and D. D. Pretzer, Phys. Rev. **139**, A256 (1965).

[9]H. D. Hagstrum, J. Res. Natl. Bur. Stand. (U.S.) A **74**, 433 (1970).

[10]M. Erbudak and T. E. Fischer, Phys. Rev. Lett. **29**, 732 (1972).

[11]F. G. Allen and G. W. Gobeli, J. Appl. Phys. **35**, 597 (1964).

[12]G. Heiland and H. Lamatsch, Surf. Sci. **2**, 18 (1964).

[13]W. Bäuerle, W. Mönch, and M. Henzler, J. Appl. Phys. **43**, 3917 (1972).

[14]T. E. Fischer and P. E. Viljoen, Phys. Rev. Lett. **26**, 1475 (1971).

[15]R. Smoluchowski, Phys. Rev. **60**, 661 (1941); see also C. Herring, *Metal Interfaces* (Am. Soc. Metals, Metals Park, Ohio 1952), p. 1.

[16]J. J. Lander and J. Morrison, J. Appl. Phys. **34**, 1403 (1963); J. J. Lander, Surf. Sci. **1**, 125 (1964).

[17]P. W. Palmberg and W. T. Peria, Surf. Sci. **6**, 57 (1967).

[18]D. Haneman, Phys. Rev. **121**, 1093 (1961).

Model Pseudopotential Calculations of the Electronic and Bonding Properties of Group-IV Elements

Carmen Varea de Alvarez*† and Marvin L. Cohen*

Department of Physics, University of California, Berkeley, California 94720

and Inorganic Materials Research Division, Lawrence Berkeley Laboratory, Berkeley, California 94720

(Received 14 February 1973)

We have calculated the band structure and electronic charge densities as a function of position in the unit cell for several two-parameter pseudopotential models for group-IV elements. This was done in an attempt to understand the relationship between charge density and band structure in crystalline diamond-structure semiconductors. We have found that by changing only one parameter in the pseudopotential we can simulate the properties of the group-IV semiconductors.

I. INTRODUCTION

The group-IV elements carbon, silicon, germanium, gray tin, and lead form a very interesting series. The four atomic valence electrons for these elements are in the $s^2 p^2$ electronic configuration. For the crystalline state, in the cases of C, Si, Ge, and Sn (but not Pb), the formation of sp^3 hybrid orbitals gives the strongest bonding

overlap and this is the most stable configuration in the crystalline state. The sp^3 orbitals give rise to four equivalent tetrahedrally coordinated bonds and this bonding results in the diamond structure for these crystals. In this group, the bond energy is a decreasing function of the atomic number; carbon has a very strong bond, while gray tin is only stable at low temperatures and undergoes a phase transformation at 292 °K to metallic white

tin. Lead crystallizes in the fcc structure and is metallic.

The optical properties of these crystals can be correlated to their bonding properties. The fact that empirical-pseudopotential-method[1] (EPM) calculations on charge density[2] predict the bonding trends in tetrahedrally coordinated crystals so well indicates that trends in the imaginary part of the dielectric function $\epsilon_2(\omega)$ (which is the input in EPM calculations) contain the relevant information about how these crystals are bonded. In diamond-type crystals $\epsilon_2(\omega)$ consists essentially of two main peaks, one at low energies (energy E_L) associated with transitions at the L point of the Brillouin zone (BZ) and another prominent peak at higher energies (energy E_X) associated with a region around the X point of the BZ (actually this structure is associated with Σ and Δ). Phillips and Van Vechten[3] have pointed out that the strongest bond is expected when all optical oscillator strengths are concentrated at one energy gap. Furthermore, for a fixed average gap E_g, if one part of the conduction band is close to the valence band, appreciable mixing of the valence band with the conduction band is expected, so that a measure of the dehybridization of the wave function is given by $E_X/\bar{E}$ where $\bar{E}$ is an average of E_L and the energy of the smallest direct gap.

Two important features are essential when doing an EPM calculation: (1) the nearest-neighbor distance, which increases in going from C to Pb and (2) the pseudopotential, which depends on the element of interest. These features raise an interesting question: Is it the change in nearest-neighbor distance d that is responsible for the marked differences between these materials, or is it the different effective potential that the electrons feel outside the core which produces such differences? A partial answer comes from pressure experiments. The application of hydrostatic pressure is expected primarily to decrease d. What one observes in this case is an increase in the average direct gap and a trend toward metallization. These effects are contradictory when compared with changes in d between different elements; i.e., d increases going from C to Sn. Therefore, results based on hyrostatic pressure alone cannot explain the observed trends in the group-IV materials.

To investigate the dependence of the properties on the potentials used, we have calculated the band structures and electronic charge densities in the diamond structure for three model pseudopotentials using only two parameters to specify the pseudopotentials. One of these parameters was kept constant, while the other was chosen to give the band structure of a 1-eV gap semiconductor like Ge, a zero-gap semiconductor such as Sn, and

a band structure with overlapping bands having metallic properties. We have also calculated the band structure and charge density in the Thomas-Fermi approximation for a pseudopotential appropriate to Ge. All through this work the lattice constant used was that of Ge.

A similar approach has been taken by Heine and Jones.[4] They investigated the dependence of the band structure of diamond-type semiconductors on the pseudopotential form factors $v(\sqrt{3})$ and $v(\sqrt{8})$ (the same ones used in this work). From their calculations using perturbation theory, they suggest that when the pseudopotential form factor $v(\sqrt{8})$ is zero, the bonding charge is zero. Our charge density calculations show that both the criteria of Phillips and Van Vechten (essentially $E_L \to 0$) and Heine and Jones [$v(\sqrt{8}) \to 0$] are equivalent and give complete dehybridization. This explains in part why Pb does not crystallize in diamond structure since the Heine and Animalu $v(\sqrt{8})$ for Pb is negative.

II. PSEUDOPOTENTIAL METHOD

In this approximation, the crystal is considered as a collection of N spherically symmetric ions located at the lattice sites. The ZN valence electrons do not interact with each other except in a Hartree sense, and they interact with the ions through a weak local pseudopotential $v(r)$. This pseudopotential includes the Coulomb attraction with the ions, $-Ze^2/r$ and a repulsive term near the core arising from the requirement that the valence-electron wave functions be orthogonal to the core wave functions (the highly localized core states are not solutions of the pseudopotential Schrödinger's equation, so that the pseudopotential is much weaker near the core region than the actual potential). The final contribution to the pseudopotential comes from the interaction arising from the valence electrons which can be included by using a screening function.

Once the pseudopotential is fixed, the energy bands and electronic charge density can be obtained by solving for the eigenvalues and eigenvectors of the one-electron Schrödinger equation

$$[(p^2/2m) + V(\vec{r})]\varphi_{n,\vec{k}}(\vec{r}) = E_n(\vec{k})\,\varphi_{n,\vec{k}}(\vec{r}) , \qquad (1)$$

where $\vec{k}$ is the wave vector, n the band index, and where the pseudopotential is given by

$$V(r) = \sum_{\text{ion sites}} v(\vec{r} - \vec{r}_j) . \qquad (2)$$

The crystal symmetry is easily taken into account when this pseudopotential is expanded in the reciprocal lattice. In the diamond structure, with two atoms per cell at positions $\pm\vec{\tau}$ where $\vec{\tau} = \frac{1}{8}a$ $\times(1, 1, 1)$ (a is the lattice constant), Eq. (2) becomes
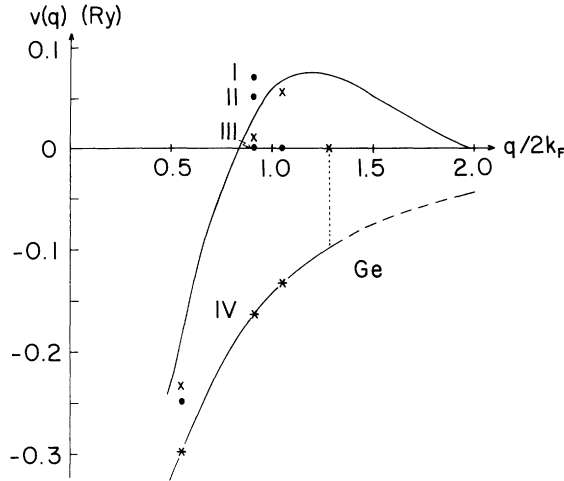
FIG. 1. Pseudopotential parameter $V(q/2k_F = 0.901)$ for models I, II, and III is shown by dots. $V(q/2k_F = 0.551)$ and $V(q/2k_F = 1.056)$ are fixed for the three models. The pseudopotential of Animalu and Heine (Ref. 6) is given by the upper solid line. The parameters of Cohen and Bergstresser (Ref. 5) are given by the crosses. Finally model IV is given by the stars connected by a solid line.

$$V(\vec{r}) = \sum_G v(\vec{G}) \cos(\vec{G} \cdot \vec{\tau}) e^{i\vec{G} \cdot \vec{r}} , \tag{3}$$

with

$$v(\vec{G}) = (2/\Omega) \int v(r) e^{i\vec{G} \cdot \vec{r}} d^3r , \tag{4}$$

where Ω is the volume of the primitive cell and G is in units of $2\pi/a$. Usually, in EPM calculations only the form factors $v(\sqrt{3})$, $v(\sqrt{4})$, $v(\sqrt{8})$ and $v(\sqrt{11})$ are allowed to be nonzero, but the structure factor $\cos \vec{G} \cdot \vec{\tau} = 0$ for $|G| = 2$ for diamond-structure materials. Therefore this method uses three adjustable parameters to fit the known energy-band features. In Fig. 1 we show the three form factors obtained by Cohen and Bergstresser[5] for Ge together with the theoretical pseudopotential of Animalu and Heine[6] and the parameters used in this work.

The pseudopotnetial curves $v(q)$ can usually be divided into two regions separated by a point where $v(q_0) = 0$ (q_0 is related to the radius of the atomic core r_0). For $q < q_0$, $v(q) < 0$ and this region represents the screened attractive Coulomb potential outside the ion cores; for the region $q > q_0$, $v(q)$ is positive and approximately represents the repulsive part of the potential arising from the orthogonalization conditions inside an effective core radius. With this in mind, one would expect to obtain all the main properties of the band structure and electronic charge density from only two form factors, each representing one of the two regions. Generally, since $q_0 \leq \sqrt{8}(2\pi/a)$, the parameters we

choose are $v(\sqrt{3}) < 0$ and $v(\sqrt{8}) \geq 0$. The actual values for the model potential we chose are given in Ry below. For model potential I,

$$v(\sqrt{3}) = -0.25, \quad v(\sqrt{8}) = 0.071 ;$$

for model potential II,

$$v(\sqrt{3}) = -0.25, \quad v(\sqrt{8}) = 0.053 ;$$

for model potential III,

$$v(\sqrt{3}) = -0.25, \quad v(\sqrt{8}) = 0.0 .$$

We have also investigated a Thomas-Fermi model with a cutoff of the potential at $q = 4(2\pi/a)$. The resulting form factors are in Ry:

$$v(\sqrt{3}) = -0.3004,$$

$$v(\sqrt{8}) = -0.1688,$$

$$v(\sqrt{11}) = -0.1338 .$$

For a given set of form factors, the Hamiltonian can be solved for the energy eigenvalues and wavefunctions $\psi_{n,k}(r)$ at many k points in the Brillouin zone. The charge density for each valence band is then given by

$$\rho_n(r) = \sum_k e \, |\psi_{n,k}(r)|^2 . \tag{5}$$

In the diamond structure there are a total of eight valence electrons per primitive cell and two valence electrons per energy band. The charge density results given in the next section are plotted in the form of contour plots in the $(1, -1, 0)$ plane, which contains an atom and two of its nearest neighbors. The density is plotted in units of e/Ω, where Ω is the volume of the primitive cell.

III. RESULTS

a. Model potential I. In Figs. 2 and 3 we show the calculated energy-band structure and electronic charge density, in the valence band, for model potential I.

Table I shows a comparison between the main energy splittings obtained by Cohen and Bergstresser[5] (CB) using three form factors, the present model using two form factors, and the experimen-

TABLE I. Comparison of the main energy gaps (in eV) between model potential I, those calculated by Cohen and Bergstresser (Ref. 5) and experiment. The energy gaps for models II and III are also given.

	$\Gamma_{25'}-\Gamma_{2'}$	$\Gamma_{25}-\Gamma_{15}$	$\Gamma_{25'}-L_1$	$\Gamma_{25'}-X_1$	$L_{3'}-L_1$	X_4-X_1
Expt	1.0	3.4	0.8	1.0	2.1	4.3
CB	1.2	3.5	0.9	1.0	2.0	3.8
I	1.0	2.1	0.41	0.34	1.74	3.5
II	0	2.20	-0.07	0.25	1.24	3.35
III	-3.08	3.4	-1.46	-0.07	-0.19	2.85

FIG. 2. Band structure for model pseudopotential I.

FIG. 4. Band structure for model II.

tal values for Ge. The main difference between
our results and those of CB occurs in the first in-
direct gap. There are smaller differences in the
higher conduction bands and even smaller differ-
ences in the valence bands. This model would pre-
dict optical properties close to those obtained by
a CB potential.

From the total charge density for the four va-
lence bands (Fig. 3) the covalent bonding is appar-
ent. The concentration of charge in the bond is a
little weaker than that calculated by Walter and
Cohen[2] using a CB potential. This is not inconsis-
tent with our model since the valence-to-conduc-
tion-band average energy gap for this model is
smaller than the one calculated by CB. Thus a
simple model pseudopotential that uses only two
parameters, one representing the screened Cou-
lomb attraction to the atoms $[v(\sqrt{3})]$, and another
that represents the repulsive orthogonalization re-
quirements $[v(\sqrt{8})]$, describes quite well the ener-
gy-band structure and bonding properties of Ge.

b. Model potential II. As the pseudopotential

form factor $v(\sqrt{8})$ is reduced, the repulsive part of
the atomic potential decreases and the s-like levels
which are more sensitive to the potential near the
atoms become more tightly bound. For a value of
0.053 Ry for $v(\sqrt{8})$ the energy of the $\Gamma_{25'}$ and $\Gamma_{2'}$
levels becomes equal, giving a band structure
similar to that of gray tin.

In Fig. 4 the calculated energy-band structure
is given and in Fig. 5 the total charge density for
the four valence bands for our second model po-
tential is shown. The energy-band structure is
actually that of a semimetal with a small overlap
of 0.07 eV from $\Gamma_{25'}$ to L_1; the first direct gap is
zero, as in the case of α-tin. Table I shows the
main energy splittings obtained in model II—all the
4-5 splittings are smaller than those of model I.
In the next paragraph we show how the changes of
the energy splittings with $v(\sqrt{8})$ are easily under-
stood from the form of the wave functions at the
bottom of the conduction band.

In a separated but related work,[7] we have cal-

FIG. 3. Electronic charge density in the (1, −1, 0)
plane for model I (summed over the valence bands).

FIG. 5. Electronic charge density in the (1, −1, 0)
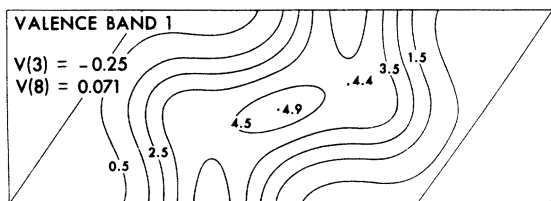plane for model II (summed over the valence bands).

FIG. 6. Electronic charge density in the (1, −1, 0) plane for the first valence band for model I.

culated the charge density for the $\Gamma_{2'}$, L_1, and X_1 states in the conduction band of Si. Our results are as follows:

(1) The charge density for states near $\Gamma_{2'}$ is highly peaked near the atoms and it is very sensitive to changes of the pseudopotential in that region in real space. It is therefore very sensitive to changes in $v(\sqrt{8})$.

(2) The charge density for states near L_1 is more "free like," but is peaked between the atoms and the antibonding site, so that they are less sensitive to changes in V_8 than $\Gamma_{2'}$.

(3) The charge density for states near X_1 is almost constant so that the energy splitting $\Gamma_{25'} - X_1$ is very little affected by changes in $v(\sqrt{8})$.

Figures 6 and 7 show the charge-density contour plots in the first valence band for model potentials I and II, respectively; the reduction of $v(\sqrt{8})$ from the first to the second model has caused a decrease in the repulsive part of the potential near the atoms, and the electronic charge tends to pile up closer to the atomic sites; the same effect is observed in band 2. Bands 3 and 4 are almost identical for models I and II; p-like bands are quite insensitive to the potential near the atoms. The only trend we observe in comparing Figs. 5 and 3 is a small trend to pile up charge closer to the atoms in model II; this tendency is also present in the charge densities of Walter and Cohen[2] going from Si to Ge to α-tin. This is mainly caused by the charge density of the first two s-like valence bands, as already discussed.

c. Model potential III. Figures 8 and 9 show the energy-band structure and total charge density in the valence band for model potential III. $v(\sqrt{8})$ is zero in this model; the energy-band structure is
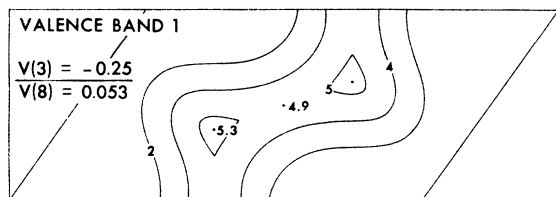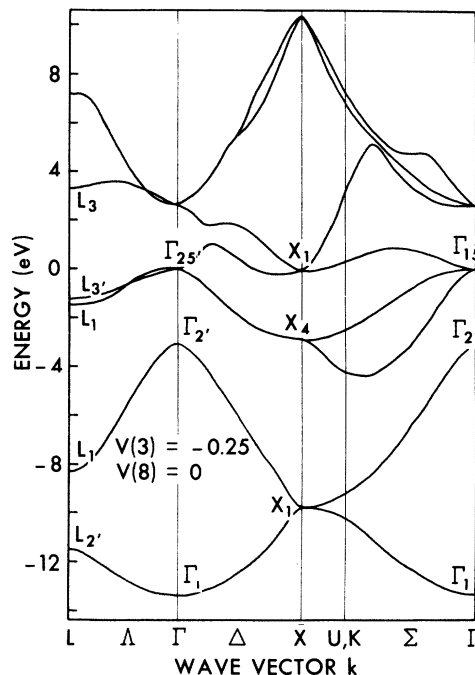

FIG. 8. Band structure for model III.

that of a semimetal and Table I includes the values of the main energy splittings.

Since $v(\sqrt{8})$ is now zero, the piling of the charge density closer to the atoms is more accentuated, as shown in Fig. 9. The charge density for valence band 3 is affected slightly, since it includes antibonding states near L_1, which is now in the valence band. The inclusion of these states affects the bonding charge for this band by about 6%, compared with the third valence band of model I. The charge for valence band 4 is again almost unaffected by the change in $v(\sqrt{8})$.

The charge density given in Fig. 9 is not precisely the charge density which our model potential would have at 0 °K. The Fermi level is somewhere between the $L_{3'}$ and $\Gamma_{25'}$ levels, so that a region around $\Gamma_{25'}$ in the third and fourth bands is unoccupied. Since the wave functions near $L_{3'}$ are very similar to those near $\Gamma_{25'}$, we do not expect that Fermi-level corrections will be very important.

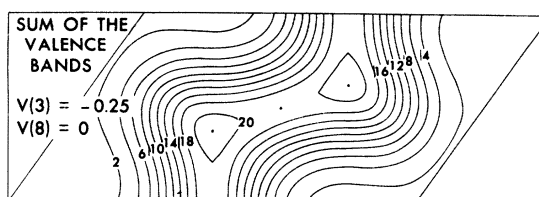FIG. 7. Electronic charge density in the (1, −1, 0) plane for the first valence band for model II.

FIG. 9. Electronic charge density in the (1, −1, 0) plane for model II (summed over the valence bands).
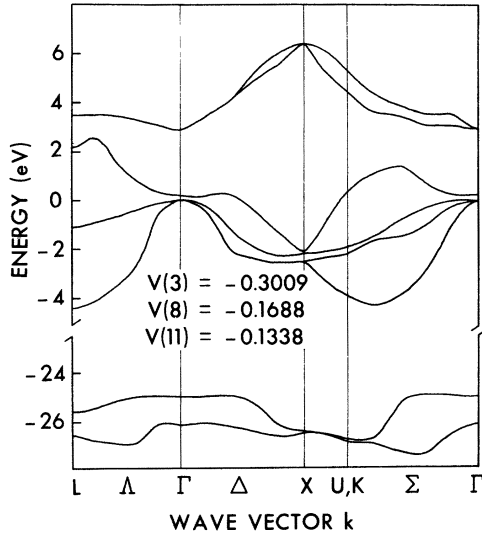
FIG. 10. Band structure for the Thomas–Fermi model.

It is interesting to compare the band structure of lead, assuming it could crystallize in the diamond structure, with the results of model III. To do this, we have calculated the band structure using the Heine–Animalu pseudopotential for lead. The lattice constant is chosen so that the nearest-neighbor distance d in our hypothetical phase for Pb is the same as the nearest-neighbor distance in its fcc phase. The justification for this choice is that when Si and Ge undergo a metallic phase transformation under pressure the nearest-neighbor distance is almost unchanged. The band structure obtained in this manner is similar to that of model III.

d. Thomas–Fermi model. In the Thomas–Fermi approximation, the pseudopotential is given by

$$v(q) = -\frac{8\pi e^2 z}{\Omega(q^2+k_s^2)} = -\frac{2}{3}\epsilon_F \frac{k_s^2}{(q^2+k_s^2)} \ .$$

Here Ω is the volume of the primitive cell, z the number of outer electrons per atom and for Ge $\frac{2}{3}\epsilon_F$ = 0.57 Ry. Since the Thomas–Fermi potential is attractive for regions even close to the cores, (no orthogonalization conditions have been imposed on the valence electrons), the electrons tend to pile up in the core region. This is reflected in the energy-band structure obtained for this model, as shown in Fig. 10. The states in the first two s-like bands are separated by a gap of 20.5 eV from the rest of the states in the valence band. These states behave essentially like core states and are not available for the formation of sp^3 orbitals. The band structure is that of a semimetal (or metal) with a large overlap. As in model III, we have not computed the effects of the

overlap on the charge density; hence the charge density shown in Fig. 11 is approximate. Nevertheless, since the charge distribution in the first two bands is highly peaked around the atoms, and bands 4 and 5 add an almost constant background to the total charge density when compared with the first two, we expect that Fermi-level corrections would not appreciably affect the total charge density. The main point is that the repulsive potential is too weak to keep the electrons outside the atoms, and the formation of sp^3 orbitals is not energetically favored.

IV. SUMMARY AND CONCLUSIONS

With a simple two-parameter model pseudopotential with one variable parameter it has been possible to simulate the variation observed in the group-IV elements. A comparison between our results for model I and model II, shows how a decrease in the repulsive part of the potential can take into account the main differences in band structure and bonding properties between Ge and gray tin. Of course, this model is too crude to include all the band-structure features of these elements, but we believe that the main trends going from Ge to gray tin are explained by a reduction in the contributions from the repulsive orthogonalization requirements $(v(\sqrt{8}))$ to the pseudopotential.

Assuming that we could construct two diamond-type crystals, one of Ge and the other of Pb, with the same interatomic distances, the major difference in their pseudopotentials, apart from screening effects, would come from the orthogonalization conditions imposed on the pseudo-wave-functions from the two different cores of Ge and Pb. That is, the main difference in the pseudopotentials would be inside an effective core radius r_0. This repulsive contribution to the pseudopotential would be mostly affected by the form factors $V(q)$ for large q, which we have included in only one variable parameter $v(\sqrt{8})$. As the positive $V(q)$ for large q decreases, the pseudopotential in real space becomes less repulsive, allowing the electrons to concentrate in a region between the real core and our effective core. If the electrons are
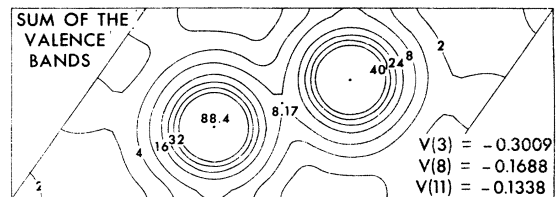

FIG. 11. Electronic charge density in the (1, −1, 0) plane for Thomas–Fermi model (summed over the valence bands).

too close to the cores, there are fewer electrons
to form the bond; hence the bonds formed when
the crystal is constructed are weak and the energy
gain in the formation of the bonds might be smaller
than the energy required to promote the electrons
from the s^2p^2 ground state to the sp^3 configuration.
The crystal would most likely change to a more
stable configuration.

With respect to the band structure and electrical
properties, since states near $\Gamma_{2'}$ and L_1 are con-
centrated close to the atoms, a decrease in the
repulsive part of the pseudopotential affects them

most. Therefore, decreasing the repulsive po-
tential would decrease the potential energy of these
states. Consequently, the first direct as well as
the first indirect gap in the band structure would
be decreased.

Because of this study using a two-parameter
model, which simulates the repulsive and attrac-
tive parts of the pseudopotential, we can under-
stand and roughly predict the dependence of the
total electronic charge density on the pseudopoten-
tial without going through a calculation of the en-
ergy-band structure.

---

[1]M. L. Cohen and V. Heine, *Solid State Physics*, edited by H. Ehrenreich, F. Seitz, and D. Turnbull (Academic, New York, 1970), Vol. 24.

[2]J. P. Walter and M. L. Cohen, Phys. Rev. B **4**, 1877 (1971).

[3]J. C. Phillips, Rev. Mod. Phys. **42**, 317 (1970); J. C. Phillips and J. A. Van Vechten, Phys. Rev. B **2**, 2147 (1970).

[4]V. Heine and R. O. Jones, J. Phys. C **2**, 719 (1969).

[5]M. L. Cohen and T. K. Bergstresser, Phys. Rev. **141**, 789 (1966).

[6]A. E. O. Animalu and V. Heine, Philos. Mag. **12**, 1249 (1965).

[7]C. Varea de Alvarez and M. L. Cohen (unpublished).